Studies of Turbulence and Transport in the Alcator C-Mod and DIII-D Tokamaks with Phase Contrast Imaging and Gyrokinetic Modeling*

M. Porkolab[1], P. Ennever[1], A. Marinoni[1], J. C. Rost[1], S. G. Baek[1], E. M. Davis[1], E. M. Edlund[1], D. R. Ernst[1], J. Hughes[1], J. E. Rice[1], and the Alcator C-Mod Team[1]; K. H. Burrell[2], J. Candy[2], R. I. Pinsker[2], G. M. Staebler[2], and the DIII-D Team[2]; B. A. Grierson[3]; G.R. McKee[4]; M. L. Reinke[5]; T. L. Rhodes[6]
[1] MIT Plasma Science and Fusion Center, Cambridge MA 02139 USA
[2] General Atomics, PO Box 85608, San Diego CA USA
[3] Princeton Plasma Physics Laboratory, PO Box 451, Princeton NJ 08540 USA
[4] Univ. Wisconsin, Madison WI 53706 USA
[5] Oak Ridge Nat'l Lab, 1 Bethel Valley Rd, Oak Ridge TN 37831 USA
[6] Univ. California, Los Angeles, 405 Hilgard Ave, Los Angeles CA 90095 USA
Email contact of main author: porkolab@psfc.mit.edu

Abstract. Experimental results are presented where the macroscopic plasma conditions were manipulated by external actuators, such as injection of medium to low Zi impurity gases with ohmic heating (Alcator C-Mod) to dilute the main deuterium ion species, or deploy a different mix of NBI and ECH heating methods (DIII-D), thus enabling us to study the resulting changes in transport and turbulence. Subsequently we were able to carry out quantitative comparisons between gyrokinetic code predictions (GYRO and GS2) and compare them with measurements of the fluctuating density spectrum based on a calibrated Phase Contrast Imaging (PCI) technique. In Alcator C-Mod, dilution by nitrogen seeding was found to decrease the ion temperature gradient scale lengths in the outer regions of the plasma where ITG modes were dominant. GYRO simulations reproduced the observed change in the energy transport with the seeding as a reduction in ITG driven transport. The PCI measured density fluctuation amplitudes also decreased substantially with nitrogen seeding. Simulations of these plasmas with the nonlinear gyrokinetic code GYRO were performed and the density fluctuations from nonlinear GYRO simulations were found to agree with the experimental PCI measurements. On the DIII-D tokamak experiments simulating the NBI heated ITER Baseline Scenario showed that added electron cyclotron heating (ECH) affected turbulent fluctuations at different scales, as measured by Phase Contrast Imaging (PCI) diagnostic. After turning off the ECH power, the intensity of fluctuations at frequencies higher than 200 kHz increased within 20 ms, due to electron modes that were enhanced by the prompt response of the electron temperature inverse scale length in the outer third of the minor radius. Such modes were observed in non-linear gyro-kinetic simulations to generate a significant transient heat flux and an inward particle pinch. In contrast, the behavior of fluctuations at lower frequencies was dictated by the slower time evolution of other equilibrium quantities such as density and flow shear. In particular, the intensity of fluctuations was observed to decrease with the mean flow shear exceeding the maximum linear growth rate of ITG modes.

1.1. Turbulence and Transport Studies on Alcator C-Mod Ohmic Plasmas.

Earlier studies of transport on Alcator C-Mod ohmic plasmas indicated that to get agreement with measured values of the ion thermal diffusivity, the main ion species deuterium charge density had to be reduced relative to that of electrons by 10-30 %, implying the presence of a few percent of intrinsic impurities with an effective ion charge of 8-10, corresponding to Oxygen like impurities [1]. The physics behind these observations was further investigated with the gyrokinetic codes GYRO [2] and TGLF [3] as well as additional experimental measurements by injecting known amounts of Nitrogen into ohmic plasmas [4]. All those measurements and simulations showed consistently that the dilution from the nitrogen seeding reduced turbulence and associated energy transport in the radial range of $0.7 < r/a < 0.9$ where strong ITG turbulence dominated transport, well above gyrobohm levels [Fig.1a]. Measured turbulence levels with phase contrast imaging agreed with the gyrokinetic code predictions based on synthetic diagnostic method [Fig 1b]. In the gyrokinetic

simulations, it was found that the dilution itself, rather than the change in *Z*eff, was responsible for the stabilizing effect on the turbulence. The physics of turbulent transport reduction in the GYRO code was the result of either an increase in the critical ion temperature gradients (mainly in the linear ohmic confinement regime), or a reduction in the ion temperature stiffness in the saturated ohmic confinement regime. The reduction in the measured turbulence levels agreed well with these theoretical predictions. Typical results are shown in Fig. 1.

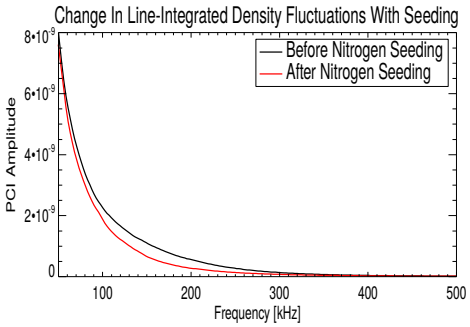

FIG. 1a. Reduction of turbulence measured by PCI with nitrogen seeding.

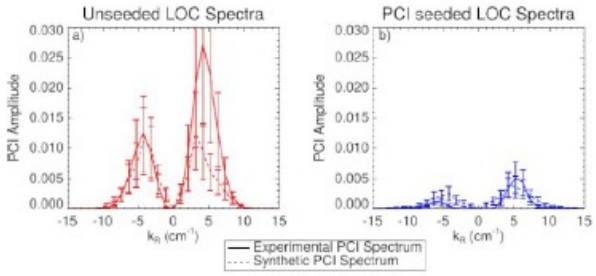

FIG. 1b. Reduction of turbulent spectrum with nitrogen seeding (Ref. 4, Fig. 10).

In recent experiments, ohmic plasmas with toroidal magnetic field B_T = 5.4T, and plasma current I_P = 1.2 MA (edge safety factor q_{95} = 3.4) at a variety of densities were seeded with neon (Z = 10) under similar conditions to the nitrogen (Z = 7) seeding experiments performed previously [4]. The neon seeding diluted the plasmas further than the nitrogen seeding did, as seen in Fig. 2. In these cases n_D/n_e was determined using a Z_{eff} computed from the neoclassical conductivity [5] and the average impurity charge determined from similar discharges with calibrated spectrometers [6], and assumes no radial variation in Z_{eff} or n_D/n_e . The neon seeding seemed to have a much larger effect on the n_D/n_e than the nitrogen did. The neon seeding significantly reduced the amount of intrinsic impurities in the plasma, so the average impurity charge is going to be very close to 10 (i.e. purely neon). The reduction in the intrinsic impurities, (B, O, Mo), could be explained by the reduction in the source of those impurities due to a change in the edge conditions (i.e. the neon seeding cools the edge and reduces the source of the intrinsic impurities). However, the reduction in the recycling argon impurity density would require a change in the particle transport. The nitrogen seeding showed similar effects on both the intrinsic and seeded impurities. This could mean that if low-Z impurities are used for divertor radiation control in fusing reactor plasmas, then it could reduce the concentration of other (perhaps more deleterious) impurities in the plasma. The fusion performance of these plasmas increased with both the nitrogen and neon impurity injection. The neutron rate, as shown in Fig. 3, increased by about a factor of two in almost every case. The neon seeding showed larger increases in the neutron rate than the nitrogen seeding, despite the decrease in the number of fusing ions being reduced more in the neon seeding case. This means that the increase in the ion temperature from the dilution was large enough to offset the decrease in the fuel ions. It could also be the case that the dilution in the inner core of the plasma (where the temperatures are the highest) was not

as large as the 0-D dilution calculation implies. The increase in the neutron rate with the seeding was despite no significant change in the ohmic input power in these discharges, as shown in Fig. 3. The total energy confinement also did not change substantially with either the neon or nitrogen seeding, as shown in Fig. 4. This is because the decrease in the turbulent energy transport was balanced by an increase in the radiated power. If the radiated power is subtracted from the ohmic power in the energy confinement time calculation, we find that the turbulent energy transport must be reduced substantially with the seeding.

The previous nitrogen seeding experiments included measurements of the ion temperature profile and those measurements showed that the ion temperature gradients increased with the impurity seeding [4], but such measurements were unavailable for the neon seeding experiments. Comparisons of the electron temperature profiles showed an increase in the normalized inverse gradient scale lengths following seeding, both at r/a = 0.8 as shown in Fig. 5 and at r/a = 0.6. This again implies that there was a reduction in the transport with the seeding. The neon seeding had a larger change in the electron temperature gradients, and a larger change in neutron rates, although this could be due to the small increase in input ohmic power with the seeding. Another result of the previous nitrogen seeding experiments was that the intrinsic toroidal velocity was being affected by the seeding [4]. A more systematic study of this phenomenon found that the intrinsic rotation in the nitrogen seeded and unseeded cases depended on the value of $n_D q_{95}$. The origin of this effect is still not well understood, and could be the result of either a change in the residual stress [6] or a change in the ion-ion collisionality [7], but a study of this phenomenon is left for future work.

1.2. Summary and Conclusions from the C-Mod Experiments.

The work presented here shows that the addition of low-Z impurities like nitrogen and neon have a net positive effect on the performance of ohmic L-mode plasmas. The neutron rate and temperature increased significantly with the seeding. This effect is not due to an increase in the ohmic power as a result of increasing Z_{eff}, since the ohmic power did not change with the seeding and the increase in the radiated power was significant. The increase in the neutron rate occurred despite the apparent reduction in the fuel ion density, so it is possible that the low-Z impurities did not penetrate into the very inner plasma core where most of the fusion reactions are occurring. Even if the low-Z impurities are only diluting the outer part of the plasma core, the increase in the temperature gradients at those locations will result in an increased core temperatures. The low-Z seeding removing other impurities in the plasma is also a beneficial result, since the higher-Z impurities in a metal walled machine will radiate more power than low-Z impurities. There is still uncertainty in how much these results extrapolate to high-performance plasmas, as well as to other reactor-relevant conditions. Low-Z impurity seeding will be necessary in metal walled reactor plasmas in order to mitigate divertor heat loads, and those impurities will likely make their way into the plasma itself, so there are already other motivations for low-Z impurity seeding in reactors. Whether or not further impurity seeding beyond the amount needed for divertor heat load control will be beneficial for transport is unclear, but there are positive effects of some amount of low-Z seeding.

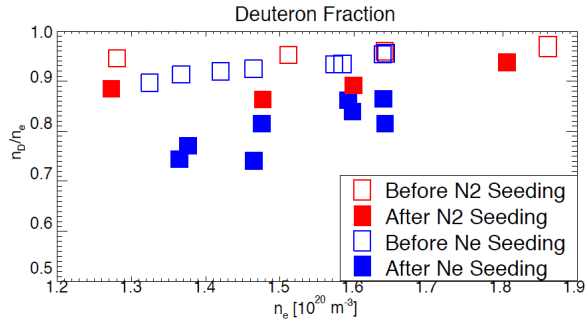

FIG. 2. Dilution of deuterium for either Ne or N2 seeding versus line average density. The Ne seeding was more effective in diluting the deuterons than nitrogen, owing to its higher charge state.

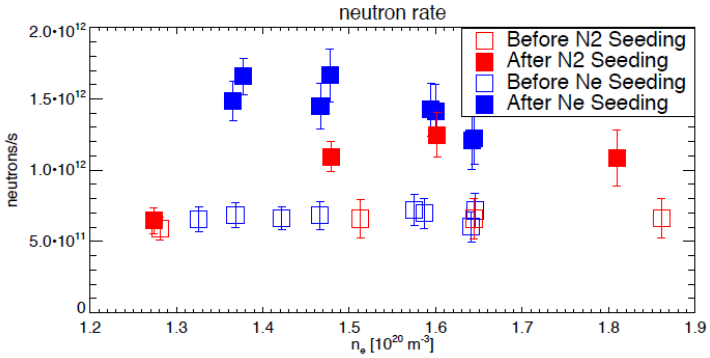

FIG. 3. Increased neutron rate observed in seeded plasmas due to increased peak ion temperature profiles dispite the radiative losses.

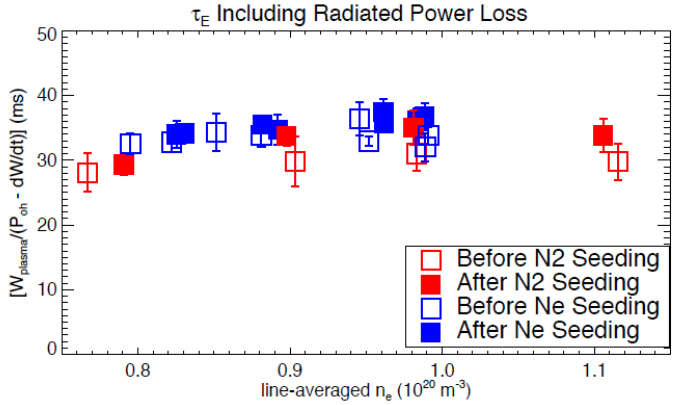

FIG. 4. Total global energy confinement time versus line average density with and without nitrogen and neon seeding. The radiated power was subtracted.

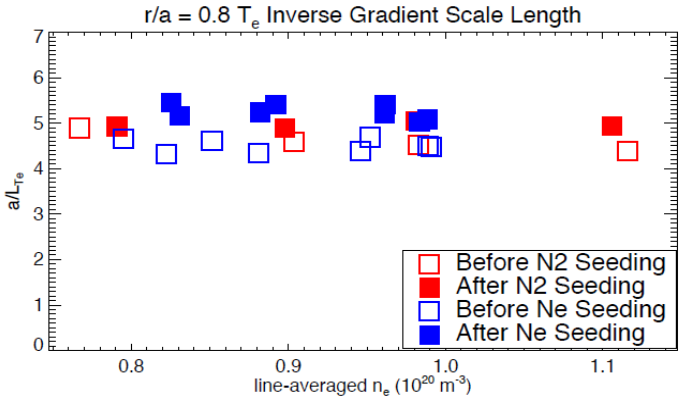

FIG. 5. The inverse electron temperature gradient scale length with and without N2 and Ne seeding, versus the line averaged density.

2.1. Effect of torque-free direct electron heating on turbulent fluctuations in DIII-D

The characterization of the so-called ITER Baseline Scenario (IBS) regime is being pursued on the DIII-D tokamak due to its importance for predicting fusion performance in ITER. Such a scenario has been recently extended to more reactor relevant regimes by carrying out experiments at low external torque and $T_e \sim T_i$, thanks to nearly balanced Neutral Beam Injectors (NBI) and to direct electron heating provided by the Electron Cyclotron Heating (ECH) system, respectively. The advantage of using ECH is twofold: first, it simulates electron heating from alpha particles generated in a burning D-T plasma, such as in ITER; second, since the location of ECH power deposition, and thus electron heating can be finely controlled, it allows one to carry out detailed studies of electron transport and related turbulence which is still poorly understood.
The IBS scenario in the experiments reported in this paper is characterized by plasma current I_p = 1.3 MA, line averaged density $n_e \sim$ 4-5 10^{19} m^{-3}, elongation κ = 1.9, top triangularity δ_T = 0.4, bottom triangularity δ_B = 0.8, normalized beta $\beta_N \sim 2$ and confinement quality factor $H_{98y,2} \sim 1$; the toroidal field was kept fixed at 1.8T, resulting in $q_{95} \sim 3.5$. A typical equilibrium can be visualized in Fig. 6, where the contour lines of the normalized poloidal flux are superimposed to the line view of the Phase Contrast Imaging (PCI) diagnostic, which is the main system used to monitor fluctuations in this paper. Plasmas are heated with 110 GHz ECH as well as with NBI, whose applied torque could be modified from co-current to balanced, and were operated in such a way as to automatically vary the injected power in order to keep β_N constant when the ECH power was turned on or off.

2.2. Effect of heating and torque on confinement and fluctuations

One of the most important goals of the experiment, and the main subject covered in this report, is to compare the impact on density fluctuations exerted by torque-free direct electron heating, i.e. ECH as a fusion alpha power simulator, to finite torque mixed electron-ion heating provided by beam sources. During the experiment, density fluctuations were monitored by Beam Emission Spectroscopy (BES) in the long wavelength range, by the Doppler Back Scattering (DBS) diagnostic in an intermediate region, and by the Phase Contrast Imaging diagnostic (PCI) that measure line averaged density fluctuations in a broad intermediate-short wavelength regime and a wide frequency bandwidth. The most important result of the experiment is a significant reduction in confinement whenever ECH is applied to replace beam power while maintaining a constant value of β_N; in particular, the NBI system had to supply only a fraction (<30%) of the ECH power. In more quantitative terms, the effect of ECH on confinement can be seen in Figure 7, which shows the time evolution of the confinement quality factor $H_{98y,2}$ as ECH power is turned off at 4.5 s. All the afore-mentioned fluctuation diagnostics measured one effect qualitatively consistent with one another, i.e. a drastic increase in the intensity of fluctuations when ECH is applied. The overall result of the measurements was reported in [8], while here we will describe in much greater detail the data and interpretation from the PCI diagnostic.
The PCI measures fluctuations in a broad range of horizontally propagating wave-numbers from 1–30 cm^{-1}, which become a combination of k_ρ and k_θ along the vertical line integral. In Figure 8 we report the power spectrum of density fluctuations for a plasma heated with beams only and with a combination of beams and ECH, at constant β_N. It can be seen that fluctuations with the largest intensity, which are within 100 kHz, are strongly enhanced by ECH, in agreement with what is observed by BES and DBS. However, at higher frequencies,

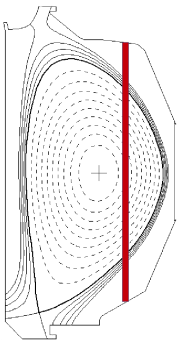

FIG. 6. (Colors on-line) Equilibrium of DIII-D discharge 154082 at 4000 ms, showing contour lines of the normalized poloidal flux. The trajectory of the PCI beam path is superimposed in red.

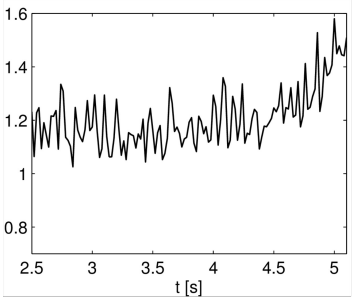

FIG. 7. Time evolution of the confinement factor $H_{98,y2}$ in DIII-D discharge #154083 where, with neutral beams power kept in β_N feedback, ECH power is removed at 4.5 s.

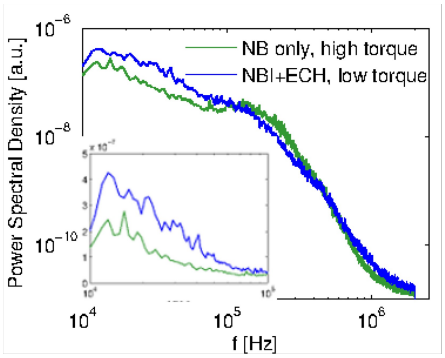

FIG. 8. (Colors on-line). Power Spectral Density (PSD) for DIII-D discharge #155198 comparing fluctuations in time intervals heated with NBI only and NBI+ECH. The results are shown both on a linear power scale (inset) and on a logarithmic power scale over a broader frequency and amplitude range.

this behavior reverses with stronger fluctuations being excited in the beam only heated part of the discharge. In order to obtain a better understanding of the low frequency response of the PCI, it is useful to examine a comparison of two similar discharges for which the main operational difference was beam torque. In Figure 9 one can see that the discharge at higher torque is characterized by fluctuations with larger frequency bandwidth and lower intensity at low frequency. This may be understood by considering that beams in a high torque configuration cause the plasma to spin faster toroidally. This produces two effects: firstly, the larger ExB shearing rate suppresses ion scale fluctuations in the low frequency part of the spectrum; secondly, a larger Doppler shift that widens the apparent bandwidth of the fluctuations to larger frequencies. The PCI diagnostic does not need a long integration time to achieve good signal, and is therefore well suited also to the study of transient phenomena. We may exploit this capability by analyzing the time evolution of density fluctuations across the turn-off time of ECH power, in a short time window during which most of the profiles are still close to values they had before the switch-off. Figure 10 shows such a comparison, where it is apparent how fluctuations at the low-end of the frequency spectrum are unaffected by the switch-off, while those at higher frequencies increase in magnitude. One of the key strengths of the PCI diagnostic is its ability to make an image of the line integrated density fluctuations onto a linear array of detectors, which allows one to extract two dimensional spectra. By analyzing the time evolution of the frequency-wavenumber spectrum of the measured signal across the ECH turn-off, it is concluded that the larger intensity of fluctuations at high frequency shown in Figure 10 is not due to an increased Doppler shift [9]. Indeed, any variation in Doppler shift correlates very well with the time evolution of the toroidal velocity of the plasmas, which varies on a much longer time scale. The larger intensity of fluctuations at high frequency is likely due to the response of the electron temperature profile to the electron heat flux variation.

2.3. Gyrokinetic Modeling

Simulations were performed with the non-linear gyrokinetic (GK) code GYRO [2], that solves the GK Vlasov-Maxwell system of equations as an initial value problem, and the gyro-

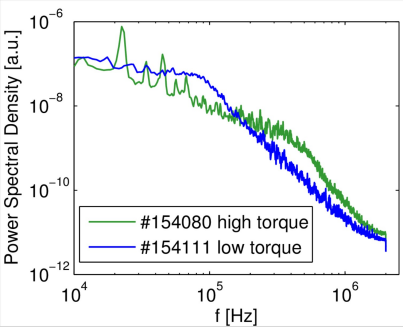

FIG. 9. (Colors on-line). PSD for beam heated sister discharges #154080 (green) and #154111 (blue) which differ in applied beam torque, leading to differences in intensity and bandwidth of fluctuations.

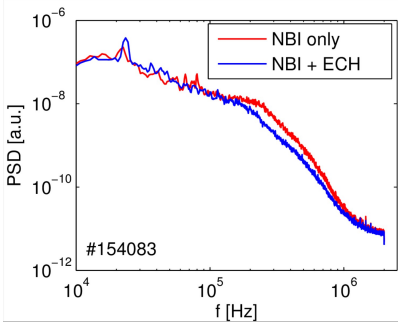

FIG. 10. (Colors on-line). PSD of DIII-D discharge #154083 across the ECH turn-off time. The intensity of fluctuations is unmodified at low frequency and increases at high frequency.

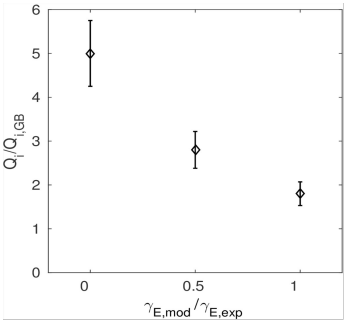

FIG.11. Effect of ExB shearing rate, from shearless to the experimental value, on the non-linear saturated ion energy flux in Gryo-Bohm units as computed by GYRO in the radial annulus 0.5 < ρ < 0.85.

fluid code TGLF [3]. The temporal evolution of confinement shown in Figure 7, and that of the measured intensity of fluctuations, can be explained by computing the radial profiles of the Hahm-Burrell shearing rate [12] in the outer half of the minor radius. While the observed shearing rate in the ECH-heated part of the discharge is well below the linear growth-rate of the most unstable mode in the ion scale region, which is where flow shear is expected to be effective, the two become quantitatively comparable in the ECH-free part of the discharge due to the toroidal spin-up. Turbulence quenching is expected to take place when the shearing rate γ_E and the maximum linear growth rate in the absence of flow shear γ_{max} satisfy the relation $\alpha\gamma_E \sim \gamma_{max}$, where α is a numerical coefficient of order unity for the case considered. Therefore, the observed reduction of the intensity of fluctuations and the amelioration of confinement are likely due to flow shear. This qualitative reasoning was confirmed by global non-linear simulations carried out in the region $0.5 < \rho < 0.8$ and in the spectral region $k_y\rho_s < 1$, which showed that the inclusion of flow shear effects lowered non-linear fluxes to values close to those from the experiment (Figure 11).

The interpretation of a line-integrated measurement, such as the PCI, can be greatly simplified by detailed modeling of the radial profiles of the dominant instabilities at play in the plasma. In particular, a first order understanding of a transient can be obtained by computing the linear growth rates in response to what caused the transient behavior. In order to understand the spectra in Figure 10, we computed the radial profile of the time evolution of the growth rate of the most unstable modes at any wavelength in the region $0.01 < k_y\rho_s < 100$. The effect of the ECH turn-off is predicted by TGLF to enhance electron scale fluctuations in the radial region $\rho > 0.6$ and for wavenumbers such that $1< k_y\rho_s < 50$. This result suggests that the increase in the intensity of fluctuations observed by the PCI diagnostic at frequencies larger than 200 kHz is due electron modes that originated from regions where the modification of the electron temperature gradient scale length in response to the heat flux variation is the largest. A comprehensive modeling of such plasmas would require the use of multi-scale simulations in order to capture the combined dynamics of ion and electron scale fluctuations [11] and are beyond the scope of this work. However, in order to obtain a reasonably accurate response of electron scale fluctuations to the ECH turn-off, non-linear local gyro-kinetic simulations were performed at electron scales at the radial location $\rho = 0.7$, where the effect of ECH on electron scale fluctuations is well visible on the linear simulations from TGLF.

The modification to the electron temperature profile is predicted to enhance the electron heat flux, with the ion heat flux being negligible, transiently. After a few energy confinement times, when profiles evolve to a new stationary state, the increased flow shear reduces the fluxes by quenching instabilities at ions scales. Interestingly, the simulations also show an increased inward particle pinch, which accounts for about 25% of the outward particle flux generated by ion scale fluctuations. This increased inward pinch might be connected to the well known ECH density pump-out effect [12].

2.4. Summary and conclusions for the DIII-D experiment

We reported on the effect of torque-free direct electron heating on DIII-D discharges in the IBS regime; in particular, we studied the behavior of density fluctuations in response to turning-off ECH power as measured with the Phase Contrast Imaging diagnostic. The variations in the characteristics of fluctuations appear to be qualitatively consistent with linear and non-linear gyrokinetic modeling. After ECH is removed and the ExB shearing rate grows over several energy confinement times, the confinement significantly increases and the low-frequency fluctuation intensity decreases. On a sub-energy confinement time scale, after turning off ECH, the PCI detects a sudden increase in the intensity of fluctuations at higher frequencies, corresponding to spatial scales between 2 and 5 cm^{-1}. Linear modeling suggests that such an effect is localized to the outer third of the minor radius, where the response of the electron temperature scale length to the heat flux variation is the largest. Non-linear gyrokinetic simulations at such scales predict larger heat flux and an inward particle pinch that might be related to the ECH density pump-out effect. Future work will attempt to quantify some of these qualitative results, by using synthetic versions of the fluctuation diagnostics in the computational turbulent transport model.

References

[1] PORKOLAB, et al., Plasma Phys. Control. Fusion **54** (2012) 124029
[2] CANDY, J., WALTZ, R.E., J. Comput. Phys. **186** (2003) 545
[3] STAEBLER, et al., Physics of Plasmas **14** (2007) 055909
[4] ENNEVER, et al., Physics of Plasmas **22** (2015) 072507 ; ibid, **23** (2016) 082509
[5] HIRSHMAN, S., et al., Nucl. Fusion **17** (2011) 611
[6] DIF-PRADALIER, et al., Phys. Rev.Lett. **103** (2009) 065002
[7] BARNES, et al., Phys. Rev. Lett. **111** (2013) 055005
[8] PINSKER, R.I., et al., EPJ Web of conferences **87** (2015) 02003
[9] MARINONI, A., Bull. Am . Phys. Soc. **60** (2015) 66 (paper CO6-6)
[10] BURRELL, K.H., Phys. Plasmas **4** (1997) 1499
[11] HOWARD, N.T., et al., Phys. Plasmas **23** (2016) 056109
[12] ERCKMANN, V., GASPARINO, U., Plasma Phys. Control. Fusion **36** (1994) 1869

Acknowledgements

Work supported by US DOE contracts DE-FC02-99ER54512 on Alcator C-Mod, DE-FC02-04ER54698 on DIII-D, both DOE FES User Facilities, and Grant DE-FG02-94ER54235 at MIT. DIII-D data shown in this paper can be obtained in digital format by following the links at https://fusion.gat.com/global/D3D_DMP.